Environmental Effects of Ashfall in Argentina from the 2008 Chaitén Volcanic Eruption

RS Martin[1], SFL Watt[2], DM Pyle[2], TA Mather[2], NE Matthews[2],
RB Georg[2], JA Day[1], T Fairhead[3], MLI Witt[2], BM Quayle[2].

[1] Department of Earth Sciences, University of Cambridge, Cambridge, UK.
[2] Department of Earth Sciences, University of Oxford, Oxford, UK.
[3] Cavendish Laboratory, University of Cambridge, UK.

Abstract

Analyses of air, water and vegetation samples collected in June 2008 offer new insights into the environmental effects of the May 2008 Chaitén eruption on Argentina, which was subject to significant ashfall between 42°S and 46°S.

Results from air filtration in the ash-affected town of Esquel (with samples analysed by gravimetry and scanning electron microscopy) show the total mass of resuspended ash in the air is well-correlated with traffic activity. However, this variation is primarily related to varying amounts of the largest particles, with little variation in the amounts of fine ash particles (i.e., d < 4 μm). This result suggests that the hazard associated with resuspended ash remains high even when traffic activity is low and the air is not visibly dusty. We estimate $PM_{2.5}$ ~ 200 μg m^{-3}, PM_4 ~ 300 μg m^{-3} and PM_{10} ~ 1000 μg m^{-3}; these concentrations far exceed WHO air quality guidelines and likely persisted for several months.

Results from water and vegetation sampling (with samples analysed by inductively coupled plasma mass spectrometry and ion chromatography) indicate that ashfall resulted in significant compositional changes in ephemeral lakes and Coirón grass (*Festuca pallescens)*. For B, Cd, Zn, Tl, Cu and Ni, there are strong linear correlations between concentrations and ash thickness (where >2 mm) in both datasets. These results suggest that the eruption of Chaitén led to significant changes in the concentrations of trace volatile elements within the environment. Analysis of vegetation samples collected in January 2009 indicates that the elevated element concentrations in Coirón grass persisted for < 8 months. These results offer insights into the environmental fate of volatile trace elements emitted during volcanic eruptions.

Keywords

Environment; Ash; Leachate; Chaitén; Patagonia; Eruption; Volcanic; Coirón

1 Introduction

1.1 The environmental impacts of volcanic eruptions

Explosive volcanic eruptions may lead to significant environmental impacts over a wide range of spatial scales. Within the "proximal" area surrounding the eruption site, the physical impacts may be immediate and devastating, due to blast waves, pyroclastic flows, lahars and volcanic bombs (Annen and Wagner, 2003). The spatial extent of these hazards and impacts is limited by the rapid cooling of volcanic ejecta and gases, and gravitational settling of the largest clasts. In contrast, the more subtle chemical impacts of volcanic eruptions may be experienced over much larger areas, as fine volcanic ash, aerosol and volcanic gas are dispersed widely by the prevailing atmospheric motions.

Recent studies have offered new insights into the distal environmental impacts of volcanic eruptions. These impacts range from the truly global scale (e.g., the climatic effects of sulphuric acid aerosols; Robock et al., 2000), to the continental scale (e.g., localized ozone holes due to halogen emissions; Millard et al., 2006), to the regional scale, just beyond the reach of the proximal volcanic phenomena, where environmental impacts are dominated by the fallout of volcanic ash (e.g. Inbar et al., 1995) and, potentially, acid sulphate deposition (Delfosse et al., 2005; Gauci et al., 2008). On the regional scale, the most significant direct impact for human health may be through the inhalation of fine volcanic ash. Particles with aerodynamic diameters $d < 10$ μm (the "thoracic" fraction) may enter the bronchi causing respiratory aggravation (e.g., triggering asthma attacks in susceptible people). The finest particles ($d < 4$ μm; the "respirable" fraction) do not impact upon the bronchi but pass into the alveolar region of the lungs potentially leading to respiratory illnesses. The two main concerns at present are crystalline silica (causing silicosis and cancers; Baxter et al., 1999) and Fe-rich ash particles (causing lung inflammation and the in-vivo production of hydroxyl radicals through the Fenton reaction; Horwell et al., 2007). The impacts of fine ash on human populations are not limited to transient ashfall events, but may persist for some months due to the resuspension of ash by winds or vehicle movements (Hobbs et al., 1983; Inbar et al., 1995; Horwell et al., 2003). Further mechanisms for toxicity may be related to compounds on the surface of the ash, which are adsorbed as volcanic gases cool and condense in the eruption column (Witham et al., 2005; Delmelle et al., 2007). The major control on the composition of the adsorbed material is likely the volatility of elements at magmatic conditions; for example, the ratio As/Ca will be higher within adsorbed material compared to the volcanic glass since As is more volatile than Ca (e.g., Aiuppa et al., 2003; Fulignati et al., 2006). Whilst the potential impacts of these adsorbed (and thus, readily leachable) compounds on human well-being are unclear, the impacts on

agriculture are better understood. Animals may take up leachable elements through the ingestion of ash, or by drinking water contaminated with ash. The greatest concerns in this respect are fluoride and sulphur, which are toxic to livestock in high concentrations (e.g., Cronin et al., 1998, 2003). Recent studies have shown that trace elements may also be transferred rapidly from ash into the environment, giving measurably increased concentrations in waters (e.g., Frogner et al., 2001; Jones and Gislason, 2008) and vegetation (e.g., Cronin et al., 1998; Watt et al., 2007; Martin et al., 2009). The effects of trace element deposition on human, animal and plant life are not well understood, although it seems likely that any detrimental impacts would be subtle in comparison to the impacts of fluoride and sulphur, and the most important effect may be the addition of nutrients. In any case, understanding these processes is crucial to understanding of the environmental fate of volcanogenic trace elements.

1.2 This work

Chaitén volcano, situated in the southern Chilean Andes at 42.8 °S, began erupting explosively on 2nd May 2008 (Lara, 2009). Prior to the eruption, the volcano comprised a rhyolitic lava dome within a 2.5 km diameter caldera, both thought to result from the only previous volcanic activity known from Chaitén, dated at 9370 ^{14}C yr BP (Naranjo and Stern, 2004). The event led to the evacuation of >5000 people from the surrounding area from settlements up to 75 km distant, and estimates of the eruption volume (~0.2 km^3 of tephra, Watt et al., 2009) suggest that it was the largest eruption globally since that of Hudson, Chile, in 1991 (Scasso et al., 1994) and the largest explosive rhyolitic eruption since Novarupta, Alaska, in 1912. The most energetic activity took place in the initial days of eruption, culminating on 6th May, although lower-level explosive activity is continuing at the time of writing (April, 2009). Ash was deposited predominantly east of the volcano, reaching the Atlantic coast of Argentina. Preliminary characterization of the ash (Horwell et al., 2008), and our own observations, show that the ash was highly angular, being composed primarily of fragmented glass (obsidian), accompanied by vesicular pumice and rare fragmented crystals. The ash is fine grained with ~5–15 vol% and 10–30 vol% in the respirable and thoracic fractions (respectively; as a cumulative percent within the d < 1 mm fraction). The ash had low crystalline silica content (~5 wt%) suggesting that that the ash is more likely to represent a respiratory hazard in terms of in-vivo hydroxyl formation or other factors than in terms of silicosis. The geography of the area affected by ashfall is characterized by lakes and mountains to the west (>71°W; termed the Patagonian Andes), with wide open plains (<71°W; termed Patagonian Plateau, or Steppe) toward the Atlantic Ocean. Human populations are concentrated in large towns in the west (e.g., Bariloche and Esquel) and east (e.g., Trelew and Rawson) with smaller, remote settlements scattered throughout the plains. The main industries within the Patagonian Andes region are

tourism and agriculture (e.g., cattle and sheep, fruit production), and these are most concentrated around the major settlements.

In the first part of this study, we present time-resolved measurements of resuspended ash concentrations in the air close to a busy road in the centre of Esquel (~100 km east of Chaitén; *pop* ~ 30,000; ash thickness at the time of sampling T ~ 10 mm) on 4th June 2008 (approximately 1 month after first ashfall). Measurements were made using air filtration and gravimetry. Several of the filters were also analysed using scanning electron microscopy (SEM) to determine the grain size distribution of resuspended ash, and to assess whether the size distribution of ash particles varies during the day. In parallel, traffic surveys were performed in order to assess whether resuspended ash concentrations are related to traffic activity (i.e., the number of vehicles passing the sampling site per unit time).

In the second part of this study, vegetation (Coirón grass; *Festuca pallescens*) and water (from shallow, ephemeral lakes) samples were collected from across the ashfall-affected region in June 2008 and analysed by inductively coupled plasma mass spectrometry (ICP-MS) for major cations and trace elements, with waters also being analysed by ion chromatography (IC) for major anions (e.g., F^-, Cl^-, SO_4^{2-}). These environmental samples were collected during fieldwork that also included the measurement and mapping of the deposit in Argentina (as described in Watt et al., 2009). Ash thickness was measured at all sites, allowing us to investigate the relationships between ash thickness and element concentrations in environmental samples approximately 1 month after first ashfall. An additional suite of Coirón grass samples were collected in January 2009 (when ash thickness had decreased by 50-90% at all sampling sites, with a similar absolute decrease in ash thickness across the region) and analysed similarly.

No major ashfall events were encountered during either sampling period (29th May – 11th June 2008 and 10th January - 20th January 2009), consistent with the lower activity of Chaitén during these periods.

2 Methodology

2.1 Field Methods

The air in Esquel was sampled between 08:00 and 19:00 (local time) on 4th June 2008 for particulates using filter packs pumped at rates of ~17 L min^{-1}. The filter pack consisted of a particle filter (Millipore, 47 mm, AAWP pore size 0.8 μm) followed by an additional filter (Whatman, 47 mm, type 41) to limit the flow rate. The filter pack was attached to a pole ~1.6 m above the ground (i.e., the height of the mouth/nose of an average female adult; Freeman et al., 1995) in the middle of a busy road through the town centre. The pump was powered by a 12V,

70 A hr car battery. For each sample a new filter was loaded and the initial flow-rate through the filter pack was measured using a flow-meter. After sampling (typically 35-50 min), the filter was removed, folded in half and placed in two layers of clean zip-lock polyethylene bags. The flow-rate was not generally measured at the end of each sampling run to avoid disturbing particles on the filter. In the one sample (04-01N) where the flow-rate was re-measured, the flow-rate had fallen from 18 L min^{-1} to 15 L min^{-1} after 3 hr of sampling. This decrease in flow-rate was mainly due to running down of the battery at the end of the day, rather than accumulation of particles on the filter. The uncertainty on the determination of the flow-rate (F) was therefore limited to the precision of the flow-meter (~10%). The total volume of air (V_A) pumped through the filter pack was estimated from the flow-rate and sampling duration (t). On the day of sampling, the wind speed remained low (< 1 m s^{-1}) throughout most of the day, increasing to ~2-3 m s^{-1} after 17:30 (local time). No rain, snow or fresh ashfall were observed at any time during the day of sampling. The ash deposit on the ground was dry to the touch and fine grained (d < 100 μm). Surveys of traffic movements past the measurement site were also taken throughout the day (except early morning and late evening when light levels were low). Traffic surveys were 7 minutes long and taken at ~30 minute intervals. Traffic was categorized as pedestrians/cyclists, cars/vans or buses/trucks. Also recorded was the number of pedestrians and cyclists wearing dust masks. Extended sampling runs were performed on 5th and 7th June (during the daytime and nighttime periods, respectively). Details of air filtration samples are given in Table 1.

Shallow ephemeral lakes were selected as a sampling target because: (1) these lakes can be found throughout the sampling region, (2) the lake compositions are initially that of rainwater (which has very low mineral content within the sampling area; Drago and Quiros, 1996), subject to modification by the soil, and by evaporation/dilution, and (3) the lake compositions are expected to show the most significant response to ashfall because of their high surface area / volume ratio ("contamination potential"; Stewart et al., 2006). Samples were collected from the lakes by triple-washing HNO_3-cleaned polypropylene tubes (50 ml capacity) with the sample, followed by a final filling and sealing (gloves were worn at all times to avoid contamination). No in-situ measurements (e.g., temperature, pH or turbidity) were made because of time constraints. The samples were placed in two layers of clean zip-lock polyethylene bags for transportation. Replicate samples were collected at several sites. On return to the UK, water samples were frozen until the time of analysis. Further details relating to water samples are given in Supplementary Table 1 (i.e., precise location, estimate of lake dimensions and ash thickness)

Coirón grass was selected as a sampling target because: (1) this species grows abundantly and extensively within the region (Defossé et al., 1997), and (2) earlier work has shown that grass species uptake soluble elements rapidly from ash (Rye grass; Cronin et al., 1998). To our knowledge, Coirón grass has never previously been used as a bio-indicator for trace element concentrations within the environment so the results of the present study may have broader implications. The semi-arid vegetation limits agriculture to sheep husbandry in much of the region, and Coirón grass represent an important forage species (Bertiller and Coronato, 1994; Paruelo and Golluscio, 1994; Oliva et al., 2005). The grass is also a useful model species because of its ubiquity across the sampling region. The grass was sampled by collecting ~50 g of material at each site (typically from ~5 different plants), and placing the sample into a clean zip-lock polyethylene bag. On return to the UK, vegetation samples were brushed and washed with distilled deionised water (to remove any ash from the surface of the vegetation), and oven dried. Further details relating to vegetation samples are given in Supplementary Table 2 (i.e., precise location and ash thickness)

2.2 Analytical Methods

2.2.1 Gravimetry of particle filters

Particle filters were left for 1 hr in a clean hood to equilibrate with the ambient atmosphere (22°C, 40% RH). The filters were then weighed (M_{total}) using a balance with a precision of ± 0.05 mg. The mean and standard deviation of the mass of 10 blank filters (also equilibrated for 1 hr at 22°C, 40% RH) was determined (M_{blank} = 76 ± 0.18 mg). Thus, we estimate a total uncertainty of 0.19 mg on the mass of ash ($M = M_{total} - M_{blank}$) collected on each filter. These uncertainties are small in comparison to M (i.e., 0.3 – 5 mg). M can be related to the gravimetric particulate concentration (m_g; equivalent to total suspended particles e.g., Monn et al., 1995) of the air by E1, where V_A is the volume of air sampled. We assume that other particles (e.g., soot, road and other dusts) make a negligible contribution to m_g. This assumption is reasonable given the significant amount of ash on the ground in Esquel, and is further justified by the results presented in Section 3.1.

E1 $$m_g = \frac{M}{V_A}$$

2.2.2 SEM of particle filters

A subset of filter samples (04-01 D, 04-01 E, 04-01 H, 04-01 I and 04-01 M) were also analysed using scanning electron microscopy. The instrument (FEI XL30 ESEM FEG) operates at low vacuum ("environmental" SEM) such that pre-coating of the samples was not necessary. For

each sample, 10 - 12 areas (with dimensions of ~ 200 μm × 300 μm) were imaged at 500× magnification (accelerating voltage =10 kV, beam current = 130 pA, spot size = 1.7 nm). The areas were selected randomly although all were away from the fold in the filter and all contained at least 50 particles. Particles were well separated on the filter and typically comprised < 10 % of the entire field of view. Particles were typically angular shards with low vesicularity. All imaged particles had diameters of less than ~40 μm. Particles with diameters of less than ~ 4 μm could not be reliably discriminated from the filter.

An automated sequence was devised using image analysis software (*ImageJ;* Abramoff et al., 2004) to convert greyscale SEM images into a binary image with black particles on a white background. The sequence consisted of duplication of the SEM image and despeckle (to remove high frequency variations due to signal noise and the structure of the filter), followed by manual thresholding in order to give the best visual agreement between the original and processed images. The binary images were then analysed by *ImageJ* to calculate the equivalent diameter, d, of each particle. Results obtained using the automated sequence were comparable to results obtained by manually tracing outlines of particles (for samples 04-01D and 04-01H) and all subsequent samples were analysed using only the automated sequence.

Grain size distributions are defined by a number density in log(d) space (E2A). The class-width was fixed to d log d = 1/15. To obtain $N(d)$, the differential was divided by the area fraction of filter analysed (f) and the volume of air sampled (V_A). The value of f (~0.001) was calculated by dividing the total area imaged by the total area of particle deposition (~6×10^{-4} m^2; estimated by inspection of the exposed filters). The uncertainties on $N(d)$ are mostly related to V_A so it is more convenient to use the ratio $N(d)/N(d_o)$ where d_o = 4 μm. Grain size distributions may also be defined by a volume density (E2B). If all particles are spherical, $V(d)$ simplifies as indicated. The imaged particulate mass (m_i) can then be calculated from E2C, where ρ is the mass density of the particles, assumed to be ~2500 kg m^{-3} (i.e., rhyolitic glass). The uncertainties on m_i are potentially significant due to uncertainties on V_A, particle shape and mass density (due to composition and vesicularity). However, only the uncertainties on V_A are independent allowing m_i to be calculated self-consistently for a series of samples.

E2A $$N(d) = \frac{1}{fV_A}\frac{\mathrm{d}N}{\mathrm{d}\log d}$$

E2B $$V(d) = \frac{1}{fV_A}\frac{\mathrm{d}V}{\mathrm{d}\log d} \approx \frac{\pi}{6} d^3 N(d)$$

E2C $$m_{\mathrm{i}} = \rho V_{tot} \approx \rho \int_{-\infty}^{+\infty} V(d)\, \mathrm{d}\log d$$

2.2.3 ICP-MS and IC of water samples

The water samples were thawed in a refrigerator over a period of 48 hr. A 20 ml syringe was used with a 0.2 µm minisart Sartorius particle filter which was triple washed with ultrapure Milli-Q+ water (18.2 mΩ), followed by a single washing with the sample. The syringe was then used to withdraw 20 ml of sample, which was filtered into two clean centrifuge tubes for ICP-MS and IC analysis respectively. This procedure was repeated, using a new filter for each sample.

The concentrations of major cations and trace elements (in ppb by mass) were determined by ICP-MS analysis. To each sample, 145 µl of ultra-pure (69%) HNO_3 (VWR Analar grade, quartz distilled in house) was added prior to analysis. The instrument (Perkin Elmer Elan DRCII) was calibrated using surface water standard reference materials (USGSP35, USGST167, USGST143, LGC6019, SPS-SW2; supplied as liquids) and internal standards (10 µl of 1 ppm Rh, Re and In). Blank values were assessed with ICP-MS analysis of Milli-Q+ stored in the polypropylene tubes and filtered (as for the samples); these showed negligible concentrations of all reported elements in comparison to sample concentrations. Uncertainties are calculated as one standard deviation of the recovery with repeated analysis (n=6) of the five standards: As (8%), B (5%), Ba (3%), Ca (6%), Cd (9%), Co (3%), Cs (1%), Cu (10%), Fe (22%), K (4%), Mg (6%), Mn (3%), Mo (5%), Na (7%), Ni (3%), Rb (1%,), Sr (4%), Tl (6%), Zn (8%). A few elements with certified concentrations in the reference materials are not reported because of poor recoveries or high concentrations in the blanks. The concentrations of major anions (in ppb by mass) were determined by IC analysis. The instrument (Metrohm IC 861) was calibrated using synthetic standard reference materials (FLUKA/89886). Uncertainties are calculated as one standard deviation of the recovery with repeated analysis (n=3) of the three standards: F^- (1.5%), Cl^- (1.6%) and SO_4^{2-} (2.0%). The concentration of the reported ions in the blanks was negligible.

2.2.4 ICP-MS analysis of vegetation

The vegetation samples were inspected and ~10-15 healthy green blades from each sample were passed for further processing. The blades were ground using a rotary mill for 25 min at 250 rpm in sealed agate vessels. The ground material was then sieved at 1 mm and the fine powder was retained. Approximately 50 mg of each powder was weighed into clean vials and digested with 3 ml ultra-pure (69%) HNO_3 (VWR Analar grade, quart distilled in house) for 48 hr at 110°C, with 2 ml H_2O_2 (VWR Analar grade) added after the first 24 hr. After 48 hr, the digests were triple-washed with Milli-Q+ into a centrifuge tube and made up to 12 ml. The

digests were then centrifuged at 5000 rpm for 5 min to remove any remnant solids. Using a clean pipette, 5 ml of the digest was transferred to a second centrifuge tube and made up to 14 ml with Milli-Q+.

The concentrations of elements in each sample (in ppm by mass) were determined by ICP-MS analysis. For June 2008 samples, the instrument (Perkin Elmer Elan DRCII) was calibrated using plant standard reference materials (NIST1573a, NIST1570a, NIST1547, NIST1567a and BCRCRM281; supplied as powders) and internal standards (0.1 ml of 1 ppm Rh, Re and In). Uncertainties were calculated as one standard deviation of the element concentrations with repeated analysis (n=9) of the standards. For January 2009 samples, the instrument (Thermo-Finnegan Element 2 HR-ICP-MS) was calibrated using plant standard reference materials (NIST 1573a, NIST1547 and BCRCRM281) and internal standard (0.1 ml of 0.5 ppm In). Uncertainties were calculated as one standard deviation of the element concentrations with repeated analysis (n=4) of sample A11. Uncertainties for June 2008 and January 2009 samples were, respectively: Al (10%, 16%), As (8%, 24%), B (14%, n. a.), Ba (9%, 17%), Ca (9%, 9%), Cd (13%, 20%), Co (7%, 17%), Cu (9%, 14%), Fe (8%, 16%), K (8%, 12%), Mg (7%, 12%), Mn (8%, 11%), Mo (15%, 12%), Na (14%, 13%), Ni (6%, n. a.), Pb (8%, 6%), Rb (8%, 11%), Sr (9%, 9%), Tl (11%, 17%) and Zn (7%, n. a.). A few elements with certified concentrations in the reference materials are not reported because of non-linearity in the calibration or high concentrations in the blanks (i.e., solutions prepared identically but without the addition of powder). The uncertainties were typically 5-10% larger for the January 2009 samples, perhaps reflecting minor heterogeneities within the powdered samples (i.e., A11).

3 Results and Discussion

3.1 Airborne particulate matter

Figure 2 shows the variation in gravimetric particulate mass (m_g) throughout the day in Esquel on 4th June 2008, along with uncertainty bars (for one standard deviation; calculated using standard propagation of error formula and E1). Also shown are results from the traffic survey, presented as vehicle or pedestrian movements per minute, with some scaling for clarity. The gravimetric particulate mass peaks at ~10.30 and ~18.30, with the later peak being larger. Traffic survey results show similarly timed peaks indicating that the variation in m_g can be explained (at least partially) by variations in traffic activity. The large peak in m_g at ~18.30 reflects both high traffic activity and increased wind speed (i.e., < 1 ms^{-1} before 17:30 and ~2-3 ms^{-1} after 17:30). The peaks in m_g are also consistent with our field observations of when the air was visibly most dusty. The variations in traffic movements of small (i.e., cars/vans) and large (i.e., buses/trucks) motor vehicles are similar. Hence, it is not possible to assess which type of

vehicle had the greatest effect on m_g; during the course of sampling, all types of motor vehicles were observed to generate visible plumes of dust. These results show that the variations in m_g correspond well with visual observations, such as traffic activity, wind strength and the dustiness of the air. The proportional relationship between m_g and traffic movements was also found on Montserrat at much lower traffic activity (Horwell et al., 2003). The gravimetric particulate mass cannot be calculated for samples taken on 5th and 7th June since V_A is not known; however, the finding that M was ~ 4× greater over the day-time period (5th June) than the night-time period (7th June) (Table 1) is consistent with our findings that m_g is controlled primarily by traffic activity (however, the wind speed was not monitored during these periods so we cannot exclude greater wind speeds on 5th June). The peaks in m_g also correspond with peaks in pedestrian traffic, meaning that the exposure of humans to resuspended ash was maximised. The usage of dust masks varied throughout the day (0 – 30%; shown on Figure 2) but this variation did not follow m_g (although the data is noisy). At the time of sampling it was notable that the main factor influencing the variation in the usage of dust masks appeared to be the daily routines and attitudes toward mask usage of different groups of people. For example, the usage was particularly poor amongst children; this may relate to the limited availability of small masks, or be because of negative attitudes toward wearing the masks. In contrast, almost all cyclists were observed to be wearing dust masks, potentially reflecting the exposure of cyclists to the more concentrated plumes of ash (i.e., $>m_g$) created behind vehicles. People sweeping ash from the pavements were also observed to be wearing dust masks. These observations perhaps suggest a good awareness of the hazard associated with short exposures to very high concentrations of ash (i.e., $>m_g$), but not of extended exposures to more moderate concentrations (i.e., m_g).

Figure 3A shows the scaled number density, $N(d)/\ N(d_o)$ where d_o = 4 μm, for the particle filter samples analysed using SEM. In addition to removing any uncertainties on f and V_A, scaling also enables comparison of the size distribution of resuspended ash with that of the "source" ash deposit, which was collected from the ground and analysed by laser diffraction (Watt et al., 2009). Figure 3A shows that the size distributions for resuspended ash are steepened, to varying extents, relative to the size distribution of the ash deposit, with the resuspended ash having significantly fewer of the largest particles. The values of $N(d_o = 4\ \mu m)$ are approximately comparable between samples (Table 2) indicating that the concentrations of the finest particles do not vary significantly throughout the day, despite large variations elsewhere in the particle size spectrum. By extrapolation, we may further predict that the scaled number density for the resuspended ash samples and the ash deposit are approximately equivalent for $d < 4$ μm. The striking similarity between pairs of samples taken close in time adds confidence in the size

distributions. Figure 3B shows the scaled volume density, $V(d)/\ V(d_o)$ where d_o = 4 μm, for the particle filter samples analysed using SEM. All samples except 04-01M show that volume is concentrated within the d < 10 μm range. For 04-01M, V_{tot} may be underestimated due to the presence of large particles which were not imaged. However, $V(d)$ for the ash deposit has a maximum at ~ 75 μm (Watt et al., 2009) so the potential for further increase in $V(d)$ above ~40 μm for 04-01M is limited.

These results suggest that variation in m_g (Figure 2) is mostly due to variation in the shape of the size distribution, rather than a uniform scaling of $N(d)$ (which would be the simplest explanation for why m_g is proportional to the number of traffic movements). In rural settings, the main process by which small particles are resuspended is through saltation bombardment (Shao et al., 1993; Wang et al., 2008). In this process, large particles (d > 100 μm) are temporarily lofted by wind-driven aerodynamics. The maximum height reached by the saltating particles is on the order of ~0.01-0.10 m (Wang et al., 2006). When the saltating particles return to the ground, the impact leads to an efficient transfer of kinetic energy to small particles (d < 20 μm) which are then resuspended. In this setting, the direct re-suspension of small particles is a minor process due to cohesive forces between particles (although these are disrupted by saltation bombardment). However, the situation in urban environments (e.g., Esquel) may well be different as an important factor affecting m_g (at least, when the wind speed is low) appears to be the number of traffic movements. The most straightforward mechanism that explains our results is direct resuspension of ash particles by the transfer of kinetic energy from the wheels of the vehicle to particles on the ground (leading to disruption of intra-particle cohesive forces). The size distribution of suspended particles is steepened over time due to differences in the settling velocities between particles of different sizes; the settling velocities of ash particles with d = 1, 10 and 100 μm are ~100 μm s^{-1}, 10 mm s^{-1} and 1 m s^{-1} (respectively; Hinds et al., 1999). Hence, an increased number of resuspension events (e.g., increased traffic activity) would inhibit steepening by sustaining the concentration of the largest particles. The relative magnitudes of the settling velocities are such that the concentrations of large particles will respond very quickly to changes in traffic movements, whilst the concentrations of small particles are not so variable. Hence, $N(d_o$ = 4 μm) would not be expected to correlate well with traffic movements at the time of sampling since $N(d_o$ = 4 μm) is also affected by traffic movements over the preceding period of several hours (e.g., the relatively high value for 04-01 H may reflect carry-over from the morning peak in traffic activity).

Results from experimental and theoretical studies suggest that $N(d)$ would decrease with height as a power-law or exponential function (e.g., Wang et al., 2008 and references therein) and that the rate of decrease may be greater for large d. Close to the ground (but above the saltation

layer), the size distribution may be enriched in the largest particles relative to the ash deposit because the smallest particles are more significantly distributed through the vertical column (Horwell et al., 2003). Although the variation in $N(d)$ with height was not investigated in the present study, we note that the calculated parameters (e.g., m_g, $N(d)$, $V(d)$, V_{tot}) are valid only for ~1.6 m above the ground, and may be significantly greater at lower heights (e.g., at 0.7 m; the height of the mouth/nose of average 2 yr old). This factor (along with our observations of mask usage) suggests that the distribution of small masks suitable for children should be a priority for hazard mitigation.

Figure 4 shows a comparison of the gravimetric particle mass, m_g, and the imaged particle mass, m_i (calculated using E2B-C; Table 1). The uncertainty on m_i was estimated as 10% based on uncertainties on V_A. As discussed, additional uncertainties on m_i are not independent for a series of samples. The gravimetric and imaged particle mass are shown to be proportional, verifying our methodology. Furthermore, the gradient has a value (i.e., 1.5) close to unity indicating that over- or under-estimation of m_i was minor (e.g., if we had assumed particles were cubic rather than spherical, the gradient would be 0.75). Our comparison reveals a non-zero intercept of ~ 410 μg m^{-3}, which we interpret as the mass of particles with d < 4 μm since particles in this size range were not quantified through imaging. Note that if m_i for 04-01 M was indeed underestimated the effect would be to increase the intercept on Figure 4. The linear relationship between m_i and m_g indicates that the < 4 μm fraction makes a similar contribution to m_g in all samples (within uncertainty), consistent with earlier results for $N(d_o$ = 4 μm). In order to estimate the aerodynamic diameters (d_A) of particles, we assume that all particles are spherical with mass density ρ = 2500 kg m^{-3}, giving d_A equal to ~1.6× the equivalent diameter, d (i.e., $d_A = d$ $\sqrt{(\rho/1000)}$; Hinds, 1999). Thus, $PM_{2.5}$, PM_4 and PM_{10} correspond to the mass of particles with equivalent diameters of < 1.6 μm, < 2.5 μm and < 6.3 μm, respectively. Integration of the scaled volume density for the ash deposit suggests that of the total volume in the < 4 μm fraction (i.e., ~ 410 μg m^{-3}), ~70% lies in particles with d < 2.5 μm, and ~40% in particles with d < 1.6 μm. Integration of $V(d)$ for the resuspended ash suggests that of the total volume in the > 4 μm fraction, a proportion corresponding to ~ 500 μg m^{-3} (for all of the analysed samples) lies in particles with 4 μm < d < 6.3 μm. If we make the approximation that the scaled volume density for resuspended ash and the ash deposit are equivalent for d < 4 μm, then we estimate $PM_{2.5}$ ~ 200 μg m^{-3}, PM_4 ~ 300 μg m^{-3} and PM_{10} ~ 1000 μg m^{-3}, with little variation throughout the day (at least, within uncertainty and averaged over ~1 hr long sampling periods). These results suggest what whilst m_g can be estimated by visual observations, $PM_{2.5}$, PM_4 and PM_{10} (which are better proxies for respiratory hazard than m_g) are high even when the traffic activity and wind speed are relatively low. Our estimates of PM_{10} and $PM_{2.5}$ significantly exceed WHO air quality

guidelines (24 hr mean; PM_{10}: 50 μg m^{-3} and $PM_{2.5}$: 25 μg m^{-3}) indicating that concentrations of resuspended ash in Esquel reached levels which may have been detrimental to human health. Our estimate of PM_{10} is comparable to estimates of PM_{10} in other human settlements affected by volcanic ashfall (e.g., on Montserrat; Baxter et al., 1999). We observed that traces of the ash remained in Esquel in January 2009, although the air was no longer visibly dusty by this time. Hence, we suggest that the duration of exposure to exceedance levels of PM_{10} and $PM_{2.5}$ is likely to have been on the order of several months (after the first ashfall in May 2008).

A preliminary study of Chaitén ash (Horwell et al., 2008) found low crystalline silica content, suggesting a reduced health hazard relative to ash from other eruptions (e.g., Soufriere Hills, Montserrat). However, these earlier results must be taken in the context of the high concentrations of PM_{10}, PM_4 and $PM_{2.5}$ reported here, and also the possibility of further unknown mechanisms for toxicity (either related to the specific chemical and mineralogical composition of the ash, or to $N(d)$ more broadly). Whilst no relationship was found between dust mask usage and m_g, it is intuitive to suggest that amongst the people who wear the masks only occasionally, they are more likely to use them when traffic activity and wind speed are high, and the air is visibly dustier. Our results suggest an improved mitigation strategy for this group of people would be to make decisions based primarily upon the expected duration of exposure, rather than attempt hazard assessment based upon visual observations as it is the finer and thus less visible dust that presents the greatest health hazard.

3.2 Waters

Previous studies (e.g., Pedrozo et al., 1993; Diaz et al., 2007) have shown that lake waters vary between highly dilute and slightly acidic in the Patagonian Andes (e.g., mean Ca ~ 5 mg/L, Mg ~ 1 mg/L, Na ~ 2 mg/L, pH ~ 6-7; Diaz et al., 2007) to highly saline and slightly alkaline on the Patagonian Plateau (e.g., mean Ca ~ 50 mg/L, Mg ~ 30 mg/L, Na ~ 320 mg/L, pH ~ 7-8; Diaz et al., 2007). This difference is primarily due to decreasing orographic rainfall away from the Andes; from ~2500 mm/yr at the Argentina/Chile border to ~150 mm/yr on the Patagonian Plateau. This gradient in rainfall runs parallel to the gradient in ash thickness (Figure 1). To assess the environmental effects of ashfall, we must account for differences in dilution between the lakes. In order for an element to be used as a proxy for lake dilution: (1) the amount of element transferred from the soil to the lake must not vary significantly over the sampling area or depend on lake depth (i.e., the lake must not be saturated), (2) the element must not be supplied in significant amounts by the ash, and (3) the concentration of the element in rainfall must be low. A suitable candidate is Ca since this element is soluble in acidic waters but involatile at magmatic conditions (Aiuppa et al., 2003). Whilst it is known that soil compositions

trend comparably to lake compositions and become more saline on the Plateau (Diaz et al., 2007), this spatial variability has not been studied in detail. Thus, we simply interpret R^2 (i.e., the square of the correlation coefficient) of X/Ca against ash thickness to be the fraction of variability which can be explained by the ash thickness, with the remainder of the variability being due to other unexplained factors.

Figure 5A shows correlation coefficients (R) between element concentrations (normalised to Ca) in waters (X/Ca) and ash thickness at each site (T/mm). Correlations are calculated for the entire dataset (n=11) and for T > 2 mm (n=9). Replicates taken in the field are treated as independent samples. Results for element concentrations (ppb by mass) are tabulated in Supplementary Table 1. Rb, Tl, K, As, Cs, Mn, Zn, Cl, Cd, Zn, Cl, Fe, B, Cu and Ni show strong positive correlations (R^2 > 0.75) in samples with T > 2 mm. The ordering of elements is not significant due to differences in the analytical uncertainties. The strength of these correlations implies that the ambient soil and lake compositions (at least in the Patagonian Andes, where T > 2 mm) were a minor contribution (i.e., $\sim 1-R^2$) to the variability in X/Ca for a large number of elements. This result is consistent with all of the sampled lakes (at T > 2 mm) being slightly acidic prior to ashfall, ensuring that many elements adsorbed on the ash were soluble in the receiving waters. In more alkaline lakes, a greater than linear relationship between X/Ca and T might be expected as the solubility of elements on the ash would also increase with T due to acidification of the waters (e.g., Stewart et al., 2006). The weak negative correlations (e.g., Mg) are spurious, e.g., Diaz et al. (2007) show that Mg/Ca in lakes vary from 0.2 in the Patagonian Andes to 0.6 in the Patagonian Plateau (consistent with our results). In spite of the uncertainties on ambient element concentrations, the strong positive correlations between X/Ca for certain elements (Rb, Tl, K, As, Cs, Mn, Zn, Cl, Cd, Zn, Cl, Fe, B, Cu and Ni) and ash thickness indicate that these correlations are real, and reflect a causal relationship between ash deposition and water composition. Correlations between raw element concentrations and ash thickness are also strong and positive, though weaker than when the normalisation is applied. These results are consistent with those shown for deeper, permanent lakes (where T~50 cm) in Chile following the eruption of Hudson in 1991 (Weaire and Manly, 1996). The samples of Weaire and Manly (1996) were taken ~18 months after the onset of the eruption. It therefore seems likely that the presumed compositional changes in deeper, permanent lakes in the Andean regions affected by Chaitén's ashfall may persist for at least several months.

We have assumed that the correlations between X/Ca and T are due to the addition of elements into the environment by ashfall. An additional possibility is that ashfall resulted in acidification of the soils, leading to the increased solubility of certain elements (e.g., As, Cd, Cu, Pb) and the release of elements from the soil into the lakes. We suggest that this is not the general case for

the samples considered here because: (1) most of the lakes were sampled from the Patagonian Andes region where the soils are already quite acidic (Diaz et al., 2007), and (2) the linear correlations between X/Ca and *T* would require that the solubility must be proportional to $[H^+]$ rather than powers thereof, which is the more general case. Future studies of the response of soils to acidification may shed further light on this uncertainty (in particular, whether a sufficient enough amount of these elements can be released from the soil in order to explain the observations presented here).

Accepting for the moment that the measurements reflect the addition of elements into the environment, we may estimate the composition of soluble material on the surface of the ash. For two elements (i.e., Y and Z) which both show a strong positive correlation between normalised element concentrations and ash thickness, the gradient of (Y/Ca) against (Z/Ca) corresponds to Y/Z of the soluble material on the surface of the ash (Table 3; also Figure 5B for Y = K, Tl, As and Z = Rb). Furthermore, normalisation to Y/Z in the bulk ash (Watt et al., 2009) yields the following enrichment factors (where Z = Rb): As (14), Zn (10), K (2.4), Cu (1.5), Rb (1), Mn (0.28) and Fe (0.019). Note that as these enrichment factors are calculated relative to the bulk ash, differences between elements are smaller than if calculated relative to the lavas (or glass). In any case, these estimates are generally comparable with typical enrichment factors in volcanic plumes (e.g., Zoller et al., 1993; Taran et al., 1995; Aiuppa et al., 2003; Fulignati et al., 2006), with greater enrichments found for the chalcophile elements (e.g., As, Zn) than the lithophile elements (e.g., Mn, Fe). Of course, it is unlikely that the precise order of enrichments would be identical between volcanoes since enrichments will depend on factors such as the oxygen fugacity and magma temperature (which determine volatility). These results add further weight to our earlier conclusion that the variability in element concentrations in ephemeral lakes was due to the deposition of volcanic ash.

3.3 Vegetation

The mechanisms of element uptake in vegetation are complex (Kabata-Pendias, 1999), occurring through the roots, stem and leaves. Element concentrations in vegetation are an integration of air, soil and rainwater compositions over an unknown period of time. However, the precise details of uptake need not be fully known to use element concentrations in vegetation as an indicator of environmental conditions (e.g., Rossini-Oliva and Valdés, 2003; Kapusta et al., 2006; Martin et al., 2009 and others). In the present context, it is anticipated that elements are dissolved from the ash into a solution, allowing transfer of elements to Coirón grass.

Figure 6A shows correlation coefficients (R) between the concentrations of elements in Coirón grass sampled in June 2008 and ash thickness at each site (T/mm). Correlations are calculated for the entire dataset (n=40), for T > 2 mm (n=10) and for T > 3 mm (n=7). Figure 6B shows element concentrations against ash thickness for B, Pb and Cd. Results for other elements are tabulated in Supplementary Table 3A-B. Figure 6A shows that Coirón grass is an excellent bio-indicator for a range of elements, with strong positive correlations (R^2>0.7) for B, Pb and Cd and reasonable correlations (R^2>0.5) for Zn, Tl, Cu, Ni and Co. With the exception of Co, all these elements were also found to correlate with ash thickness in lake waters. As R~ 1 for B, Pb and Cd, the relationship between element concentrations in vegetation and ash thickness is approximately linear (at least for 2 mm < T < 11 mm). The result that R is comparable for T > 2 mm and T > 3 mm confirms that the application of an arbitrary cut-off (T = 2 mm) does not influence R significantly. The hypothesis that B, Pb and Cd vary in Coirón grass due to factors unrelated to ash thickness is not supported by the data because of the strength of correlation, and because the increase in B in the westernmost samples (i.e., at increased T) runs counter to the ambient environmental trend (i.e., decreasing element concentrations in soils to the west; Diaz et al., 2007). The correlations weaken if an increased range of ash thickness is considered (as found for lake compositions), because the area from which samples are drawn becomes more extensive and more heterogeneous in terms of other factors which may affect the composition of vegetation (e.g., salinity of the soil). The correlations between ash thickness and element concentrations in vegetation are generally weaker than those found for lakes. This result reflects the increased analytical uncertainties (in the analysis of vegetation; Section 2) and potentially non-linear relationships between element concentrations in vegetation and the environment due to biological fractionation (e.g., Kabata-Pendias, 1999). Figure 6B indicates that the element concentrations for T > 2 mm are within the normal range produced by other sources of variability. It therefore seems unlikely that the increased element concentrations would have any negative impacts on Coirón grass physiology, unless related to the short timescales over which the element concentrations are established. However, this vegetation was sampled during the Austral winter (outside the growth season) so the uptake of elements from the ash may have been even more significant if ashfall occurred during the summer months. The increase in element concentrations below T ~ 2 mm (Figure 6B) is consistent with increasing salinity of the soils on the Plateau (Diaz et al., 2007).

Figure 6C shows correlation coefficients (R) between the concentrations of elements in Coirón grass sampled in January 2009 and ash thickness (T/mm) as measured at the same location in June 2008. The range of "original" ash thicknesses from which the January 2009 samples were collected was 2.5 < T/mm < 6, with thicknesses in January 2009 being 0.2 < T/mm < 3. To allow

for fairest comparison between the two data sets, R for the June 2008 samples was re-calculated for the range $2 < T/\text{mm} < 6$ and shown on Figure 6C. Quite clearly, the correlations are much weaker in January 2009, indicating that elevated element concentrations in Coirón grass persisted for <8 months. The mechanisms by which elements are transferred from vegetation to the environment are poorly constrained though it seems likely that shedding and replacement (in the next growth season) and leaching by rainfall may be important processes. In any case, these results add weight to our conclusion that the variability in element concentrations in June 2008 was due to ashfall, rather than background variability.

An earlier study showed that As, Cd, Cu, Mo, Tl, Zn, Rb, Cs and K became rapidly incorporated into sweet chestnut leaves (*Castanea sativa*; Martin et al., 2009) following a minor eruption of Mt Etna, Sicily during the growth season. In the present study, we offer evidence for the rapid incorporation of B, Pb, Cd, Zn, Tl, Cu and Ni into Coirón grass following the eruption of Chaitén. Despite differences in length scales (i.e., < 30 km from the summit of Mt Etna but > 100 km from Chaitén) and processes of deposition (i.e., heavy ashfall from Chaitén but light ashfall and plume fumigation at Mt Etna), significant changes in the concentrations of Cd, Zn, Tl and Cu in vegetation were found in both studies. These elements correspond well to the elements that are volatile at magmatic conditions (Aiuppa et al., 2003; Fulignati et al., 2006). No evidence for increases in the concentration of non-volatile elements in vegetation due to volcanic eruptions was found in either study. However, increases in the concentration of the non-volatile elements may result if the soil is particularly nutrient poor; for example, Cronin et al., (1998) show uptake of Ca and Mg from ash into rye-grass grown in silica sand. Together, these studies suggest that volcanic eruptions typically lead to an increase in the concentration of trace volatile elements in vegetation over wide areas. Whilst the potential physiological effects of these compositional changes are not yet known, this result may offer new insights into the environmental fate of volcanogenic trace elements.

As discussed previously, the use of correlation coefficients in this study is limited in that the complexity of the dataset is reduced to a single explanatory variable. Additionally, the amount of an element deposited (per unit area) is dependent upon the total surface area (A_{tot}) of the ash deposited, rather than the ash thickness. Whilst the isopleth map of Watt et al., (2009) indicates that the size distribution of ash was stable toward the south-east (i.e., $A_{\text{tot}} \propto T$), there was an increase in modal grain size toward the secondary maximum (Figure 1) in the north-east (from where a few of the January 2009 samples were collected). However, allowing for this coarsening does not improve the strength of the correlations in January 2009 and so does not affect our conclusions.

4 Conclusions

The 2008 eruption of Chaitén had significant environmental effects over a wide geographical area. In this study, we combine results from air, water and vegetation sampling to offer insights into the environmental effects of ashfall in Argentina (between latitudes of 42°S and 46°S).

Results from air filtration suggest that in the urban environment the total mass of resuspended volcanic ash (i.e., m_g) is well-correlated with traffic activity. However, it appears that increases in the total mass are primarily related to increased amounts of the largest ash particles, rather than increased amounts of the fine ash particles (i.e., $d < 4$ μm). We suggest that this observation reflects differences in the gravitational settling velocities of large and small particles, such that high concentrations of the largest particles are only found when the frequency of resuspension events is large (i.e., during periods of heavy traffic). The corollary of this result is that the human hazard associated with the inhalation of fine ash particles does not vary throughout the day. Hence, the most important factor determining the hazard to individuals is the duration of their exposure. Our estimates of $PM_{2.5}$ (200 μg m^{-3}) and PM_{10} (1000 μg m^{-3}) significantly exceed WHO air quality guidelines. The duration of exposure to exceedance levels of $PM_{2.5}$ and PM_{10} was likely to have been on the order of several months.

Results from water and vegetation sampling indicate that ashfall resulted in significant compositional changes in ephemeral lakes and Coirón grass. Several elements (i.e., B, Cd, Zn, Tl, Cu and Ni) show strong positive linear correlations between concentrations and ash thickness (for $T > 2$ mm) in both sets of results. These results suggest that the eruption of Chaitén led to significant changes in the concentrations of trace volatile elements in the environment over a wide area. No evidence was found for increases in the concentration of non-volatile elements in either vegetation or water. Analysis of vegetation samples collected in January 2009 indicates that these elevated element concentrations in Coirón grass persisted for < 8 months. These results offer insights into the environmental fate of volatile trace elements emitted during volcanic eruptions.

5 Acknowledgements

This work was supported by a NERC Urgency Grant NE/G001715/1. RSM thanks Christ's College, Cambridge for a Junior Research Fellowship. TAM thanks the Royal Society for financial support. We are grateful to the municipal administration of Esquel, Gustavo Villarosa and Alfredo Fierro for facilitating fieldwork in the region. The manuscript benefited from the insightful comments of Shane J. Cronin and one anonymous reviewer.

604 **References**

Abramoff, M. D., Magelhaes, P. J., Ram, S. J., 2004. Image Processing with ImageJ. Biophotonics International, 11(7):36-42.

Aiuppa, A., Dongarra, G., Valenza, M., Federico, C. and Pecoraino, G., 2003. Degassing of Trace Volatile Metals During the 2001 Eruption of Etna. In A. Robock and C. Oppenheimer (Editors), Volcanism and the Earth's Atmosphere (Geophysical Monograph 139), American Geophysical Union, Washington, D. C., 41-54.

Annen, C., and Wagner, J.-J., 2003. The Impact of Volcanic Eruptions During the 1990s. Natural Hazards Review, 4(4):169-175.

Baxter, P. J., Bonadonna, C., Dupree, R., Hards, V. L., Kohn, S. C., Murphy, M. D., Nichols, A., Nicholson, R. A., Norton, G., Searl, A., Sparks, R. S. J., Vickers, B. P., 1999. Cristobalite in Volcanic Ash of the Soufriere Hills Volcano, Montserrat, British West Indies. Science, 283: 1142-1145.

Bertiller, M.B., and Coronato, F. 1994. Seed bank patterns of *Festuca pallescens* in semiarid Patagonia (Argentina): a possible limit to bunch reestablishment. Biodiversity and Conservation, 3:57-67.

Cronin, S. J., Hedley, M. J., Neall, V. E., Smith, R. G., 1998. Agronomic impact of tephra fallout from the 1995 and 1996 Ruapehu Volcano eruptions, New Zealand. Environmental Geology, 34(1): 21-30.

Cronin, S. J., Neall, V. E., Lecointre, J. A., Hedley, M. J., Loganathan, P., 2003. Environment hazards of fluoride in volcanic ash: a case study from Ruapehu volcano, New Zealand. Journal of Volcanology and Geothermal Research, 121: 271-291.

Defossé, G.E., Bertiller, M.B., and Robberecht, R., 1997. Effects of topography, soil moisture, wind and grazing on *Festuca* seedlings in a Patagonian grassland. Journal of Vegetation Science, 8: 677-684.

Delfosse, T., Elsass, F., and Delvaux, B., 2005. Direct evidence of basic aluminum sulphate minerals in an S-impacted Andosol. European Journal of Soil Science, 56(3): 281-286.

Delmelle, P., Lambert, M., Dufrêne, Y., Gerin, P., and Óskarsson, N., 2007. Gas/aerosol-ash

interaction in volcanic plumes: New insights from surface analyses of fine ash particles. Earth and Planetary Research Letters, 259(1-2): 159-170.

Diaz, M., Pedrozo, F., Reynolds, C., Temporetti, P., 2007. Chemical composition and the nitrogen-regulated trophic state of Patagonian lakes. Limnologica, 37: 17-27.

Drago, E., and Quiros, R., 1996. The hydrochemistry of the inland waters of Argentina: a review. International Journal of Salt Lake Research, 4: 315-325.

Freeman, J. V., Cole, T. J., Chinn, S., 1995. Cross-sectional stature and weight reference curves for the UK 1990. Archives of disease in childhood, 73(1): 17-24.

Frogner, P., Gislason, S. R., and Óskarsson, N., 2001. Fertilizing potential of volcanic ash in ocean surface water. Geology, 29(6): 487-490.

Fulignati, P., Sbrana, A., Clocchiatti, R., Luperini, W., 2006. Environmental impact of the acid fumarolic plume of a passively degassing volcano (Vulcano Island, Italy). Environmental Geology, 49: 1139-1155.

Gauci, V., Dise, N. B., Howell, G., and Jenkins, M. E., 2008. Suppression of rice methane emission by sulfate deposition in simulated acid rain. Journal of Geophysical Research, 113: G00A07.

Hinds, W. C., 1999. Aerosol Technology: Properties, Behavior, and Measurement of Airborne Particles, John Wiley, New York, 483 pp.

Hobbs, P. V., Hegg, D. A., Radke, L. F., 1983. Resuspension of volcanic ash from Mount St. Helens. Journal of Geophysical Research, 88(C6):3919-3921.

Horwell, C. J., Fenoglio, I., and Fubini, B., 2007. Iron-induced hydroxyl radical generation from basaltic volcanic ash. Earth and Planetary Science Letters, 261: 662-669.

Horwell, C. J., Michnowicz, S., and Le Blond, J., 2008. Report on the mineralogical and geochemical characterisation of Chaitén ash for the assessment of respiratory health hazard. International Volcanic Health Hazard Network (IVHNN) report (available from www.ivhhn.org).

Horwell, C. J., Sparks, R. S. J., Brewer, T. S., Llewellin, E. W., and Williamson, B. J., 2003.

Characterization of respirable volcanic ash from the Soufrière Hills Volcano, Montserrat, with implications for human health hazards. Bulletin of Volcanology, 65(5): 346-362.

Inbar, M., Ostera, H. A., Parica, C. A., Remesal, M. B., Salani, F. M., 1995. Environmental assessment of the 1991 Hudson volcano eruption ashfall effects on southern Patagonia region, Argentina. Environmental Geology, 25: 119-125.

Jones, M. T., and Gislason, S. R., 2008. Rapid releases of metal salts and nutrients following the deposition of volcanic ash into aqueous environments. Geochimica et Cosmochimica Acta, 72(15): 3661-3680.

Kabata-Pendias, A., 2001. Trace Elements in Soils and Plants. CRC Press, Boca Raton, 413 pp.

Kapusta, G., Szarek-Lukazewska, G., and Godzik, B., 2006. Spatio-temporal variation of element accumulation by Moehringia trinervia in a polluted forest ecosystem (South Poland). Environmental Pollution, 143: 285-293.

Lara, L.E., 2009. The 2008 eruption of the Chaitén volcano: a preliminary report. Andean Geology 36(1): 125-129.

Martin, R. S., Mather, T. A., Pyle, D. M., Watt, S. F. L., Day, J., Collins, S. J., Wright, T. E., Aiuppa, A., and Calabrese, S., 2009. Sweet chestnut (Castanea sativa) leaves as a bio-indicator of volcanic gas, aerosol and ash deposition onto the flanks of Mt Etna in 2005-2007. Journal of Volcanology and Geothermal Research. Journal of Volcanology and Geothermal Research, 179(1-2):107-119

Millard, G. A., Mather, T. A., Pyle, D. M., Rose, W. I., and Thornton, B. F., 2006. Halogen emissions from a small volcanic eruption: Modeling the peak concentrations, dispersion and volcanically induced ozone loss in the stratosphere. Geophysical Research Letters, 33:L19815.

Naranjo, J. A., and Stern, R. C., 2004. Holocene tephrochronology of the southernmost part (42°30'–45°S) of the Andean Southern Volcanic Zone). Revista Geológica de Chile, 31: 225-240.

Oliva, G., Collantes, M., and Humano, G., 2005. Demography of Grazed Tussock Grass Populations in Patagonia. Rangeland and Ecology Management, 58(5): 466-473.

Paruelo, J.M. and Golluscio, R.A., 1994. Range assessment using remote sensing in Northwest

Patagonia (Argentina). Journal of Range Management, 47:498-502.

Pedrozo, F., Chillrud, S., Temporetti, P., and Diaz, M., 1993. Chemical composition and nutrient limitation in rivers and lakes of Northern Patagonian Andes (39.5°-42°S, 71°W) (Rep. Argentina). Verhandlungen Internationale Vereinigung Limnologie, 25: 207-214.

Robock, A., 2000. Volcanic eruptions and climate. Reviews of Geophysics, 38(2):191-219.

Rossini-Oliva, S., and Valdés, B., 2004. Ligustrum lucidium Ait. f. Leaves as a Bioindicator of the Air-Quality in a Mediterranean City. Environmental Monitoring and Assessment, 96(1-3):221-232.

Scasso, R. A., Corbella, H., and Tiberi, P., 1994. Sedimentological analysis of the tephra from the 12-15 August 1991 eruption of Hudson volcano. Bulletin of Volcanology, 56: 121-132.
Shao, Y., Raupach, M. R., and Findlater, P. A., 1993. Effect of Saltation Bombardment on the Entrainment of Dust by Wind. Journal of Geophysical Research, 98(D7): 12719-12726.

Stewart, C., Johnston, D. M., Leonard, G. S., Horwell, C. J., Thordarson, T., and Cronin, S. J., 2006. Contamination of water supplies by volcanic ashfall: A literature review and simple impact modelling. Journal of Volcanology and Geothermal Research, 158(3-4):296-306.

Taran, Y. A., Hedenquist, J. W., Korzhinsky, M. A., Tkachenko, S. I., and Shmulovich, K. I., 1995. Geochemistry of magmatic gases from Kudryavy volcano, Iturup, Kuril Islands. Geochimica et Cosmochimica Acta, 59(9):1749-1761.

Wang, H. T., Zhang, X. H., Dong, Z. B., and Ayrault, M., 2008. Experimental determination of saltating glass particle dispersion in a turbulent boundary layer. Earth Surface Processes and Landforms, 31: 1746-1762.

Wang, H. T., Zhou, Y. H., Dong, Z. B., and Ayrault, M., 2008. Vertical dispersion of dust particles in a turbulent boundary layer. Earth Surface Processes and Landforms, 33: 1210-1221.

Watt, S.F.L., Pyle, D.M., Mather, T.A., Day, J.A., and Aiuppa, A., 2007. The use of tree-rings and foliage as an archive of volcanogenic cation deposition. Environmental Pollution 148(1): 48-61.

Watt, S. F. L., Pyle, D. M., Mather, T. A., Martin, R. S., Matthews, N. E., 2009. Fallout and distribution of volcanic ash over Argentina following the May 2008 explosive eruption of Chaitén, Chile. In press in Journal of Geophysical Research, doi: 10.1029/2008JB006219.

Weaire, J., and Manly, R., 1996. Chemical water quality studies in the Central Patagonian Region following the eruption of Volcan Hudson. Hydrobiologia, 331: 161-166.

Witham, C. S., Oppenheimer, C., and Horwell, C. J., 2005. Volcanic ash leachates: a review and recommendations for analysis methods. Journal of Volcanology and Geothermal Research, 141: 299-326.

605

606

607 Figure 1 Map of the sampling area with approximate sampling locations. Locations are
608 discriminated according to sample type (air filtration, lake or Coirón grass) and
609 ash thickness (Watt et al., 2009).

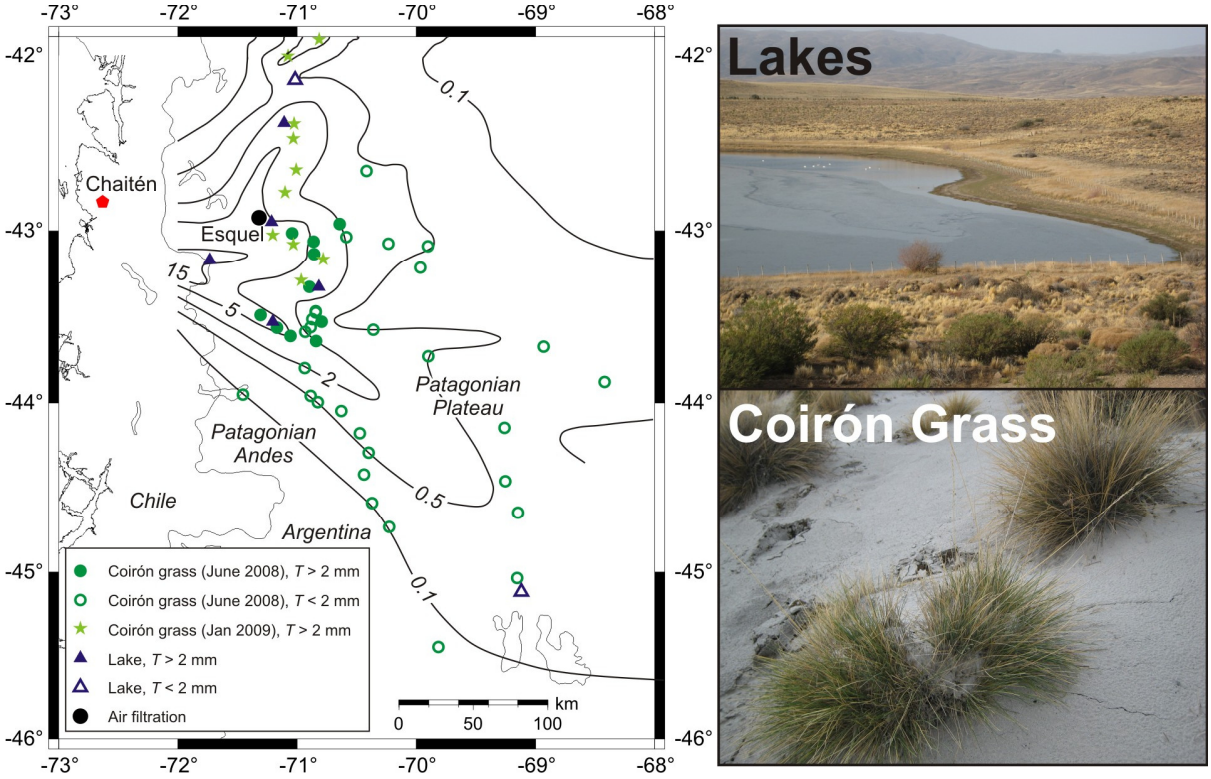

610

611

612 Figure 2 Gravimetric particulate mass (m_g) throughout the day. Also shown are traffic
613 survey results (with scaling) with dust mask usage on the same axis.

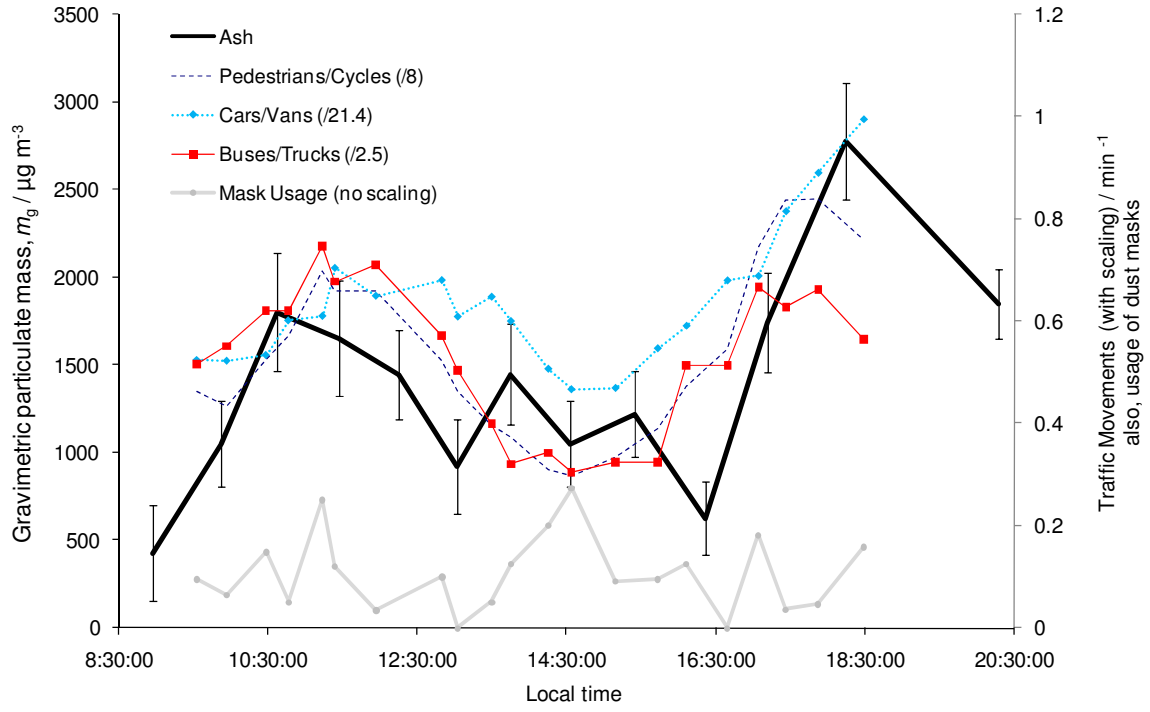

614

615

616 Figure 3A Scaled number density, $N(d)/\ N(d_o)$ where d_o = 4 µm, for air filtration
617 samples in Esquel on 4th June. Also shown is the scaled number density for
618 the ash deposit, analysed by laser diffraction (Watt et al., 2009).

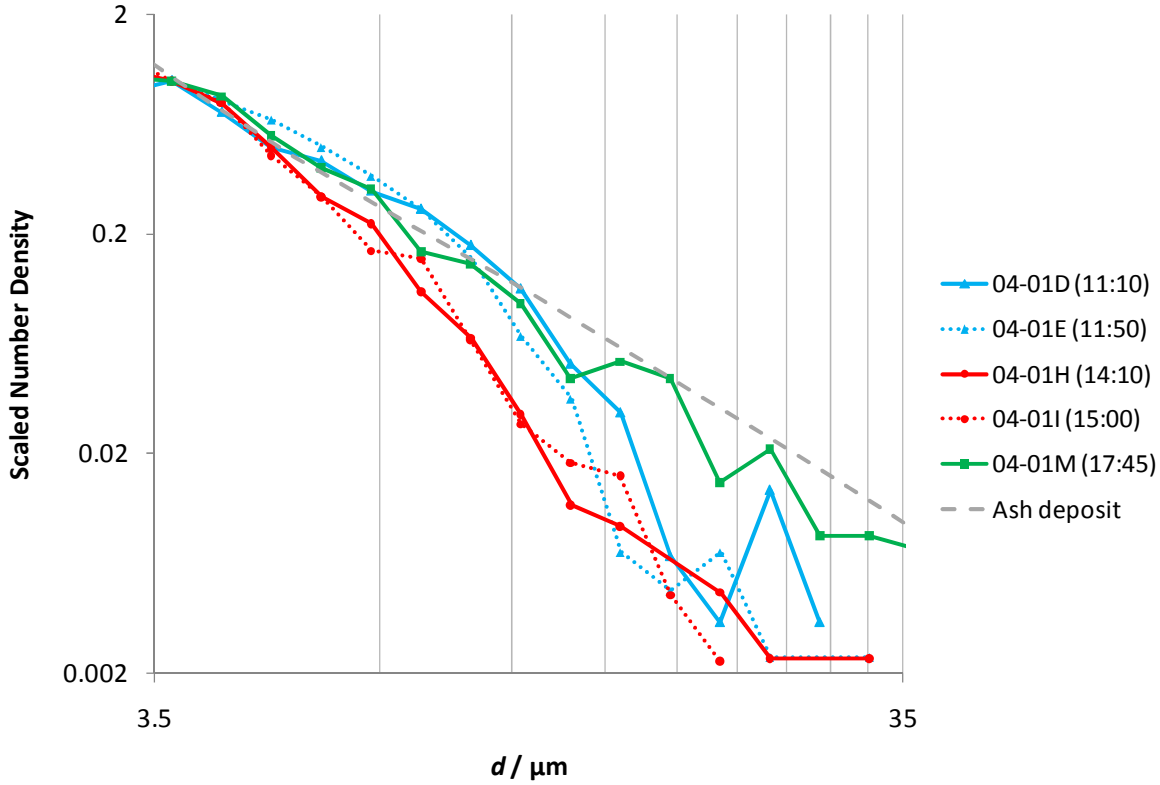

619

620 Figure 3B Scaled volume density, $V(d)/\ V(d_o)$ where d_o = 4 µm, for air filtration
621 samples in Esquel on 4th June. Also shown is the scaled number density for
622 the ash deposit, analysed by laser diffraction (Watt et al., 2009).

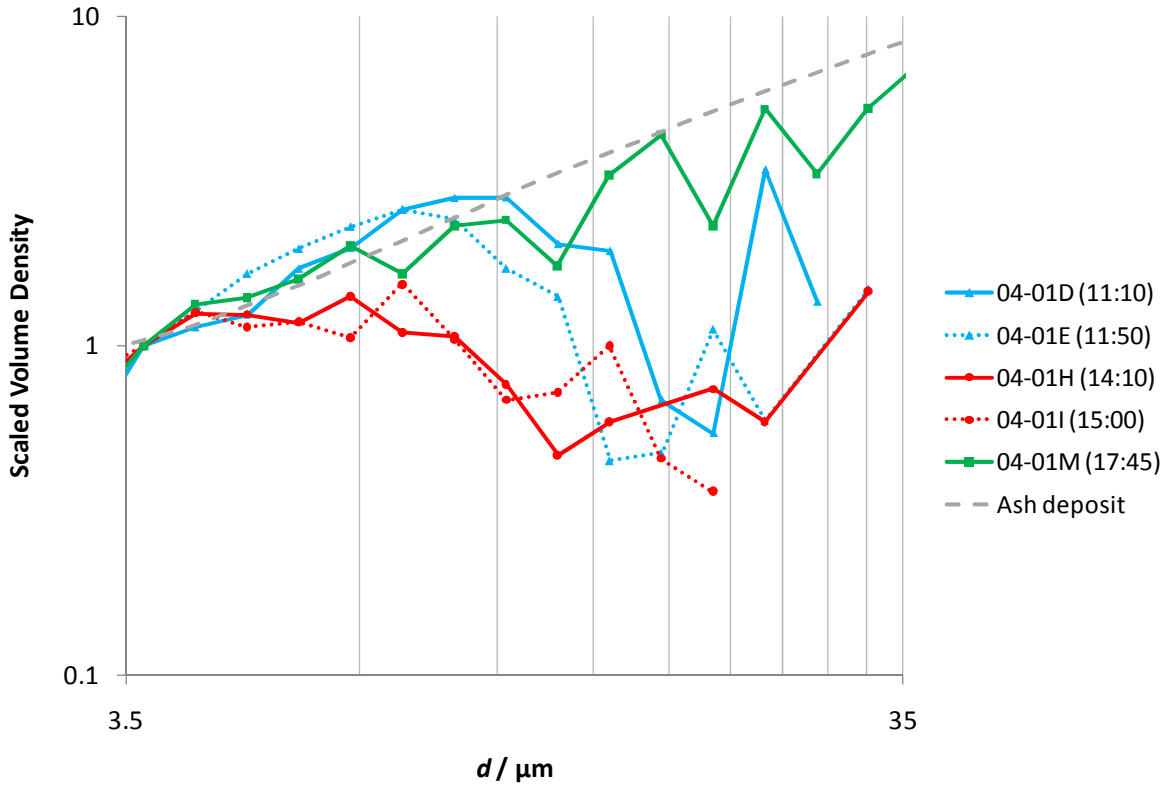

623

624

625 Figure 4 A comparison of gravimetric (m_g) and imaged (m_i) particulate mass. The
626 intercept is interpreted as the mass of particles with d < 4 μm.

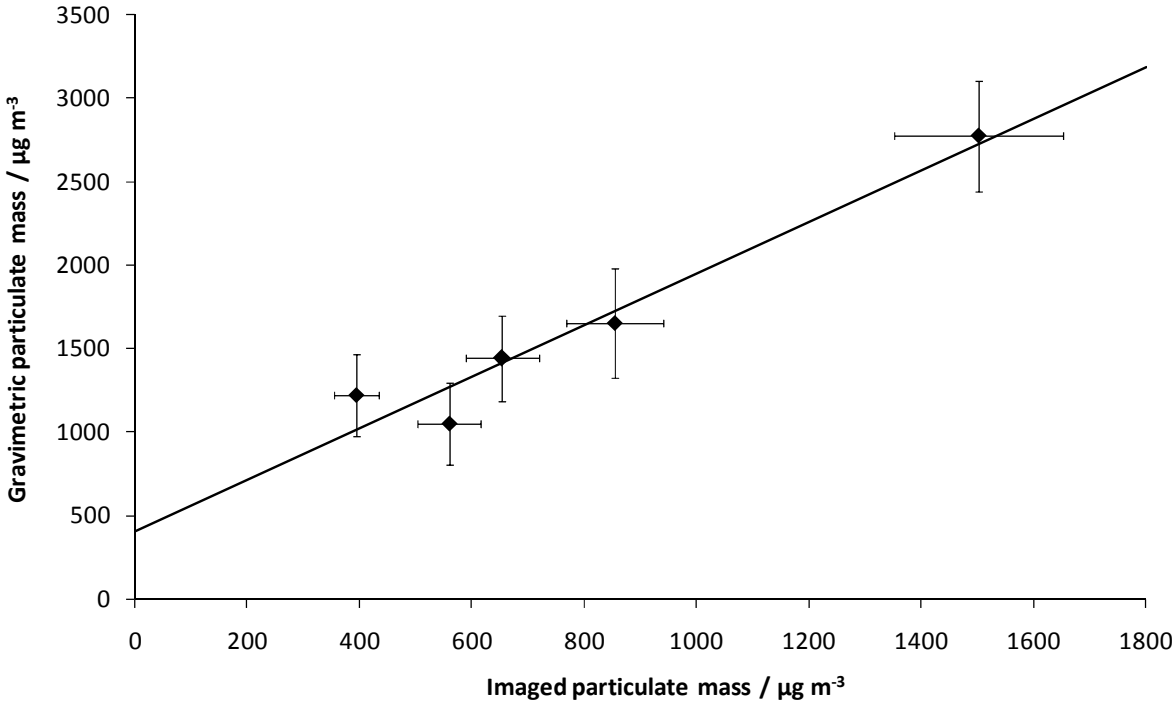

627

628

629 Figure 5A Correlation coefficients between concentrations of elements normalised to
630 Ca (i.e., X/Ca) in ephemeral lakes and ash thickness at each location (T /
631 mm).

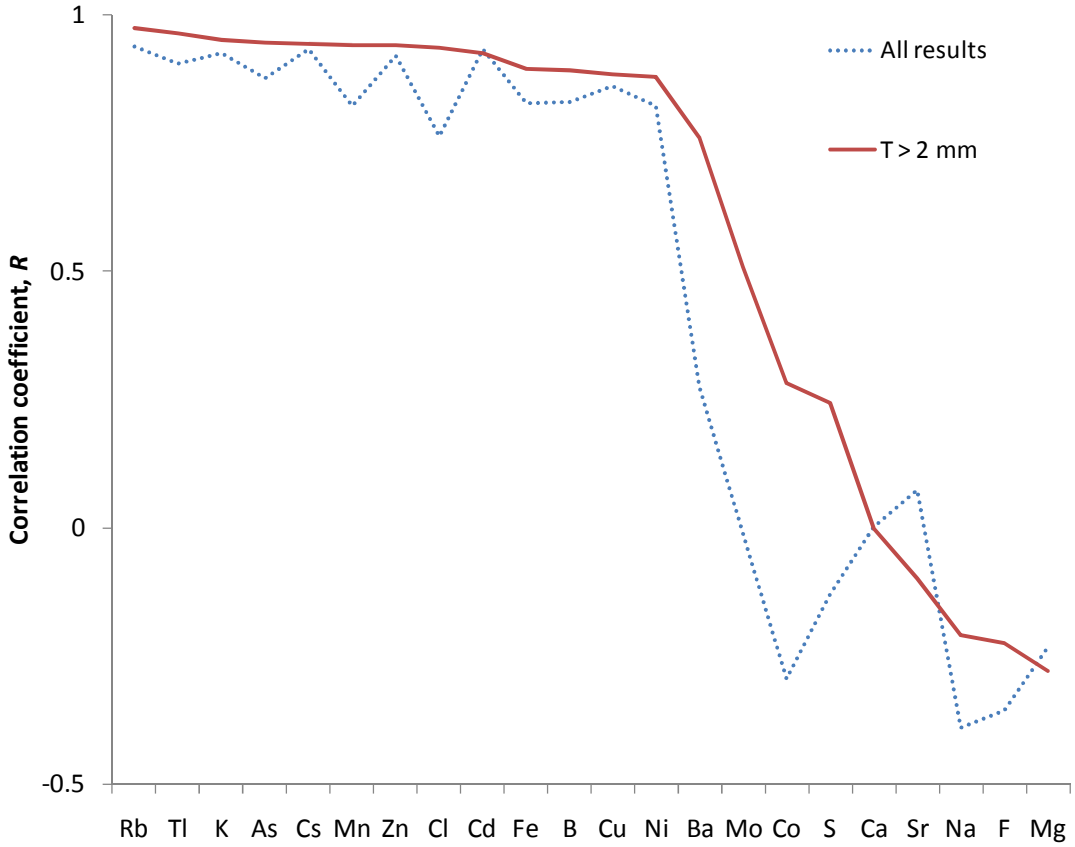

632

633

634 Figure 5B Log-log plot of (Y/Ca) where Y =K, Tl and As against (Rb/Ca). The gradient of the
635 linear fit (i.e., (Y/Ca)=m(Rb/Ca)+c) corresponds to Y/Z of the soluble material
636 available from the surface of the ash. Scaling is applied to As/Ca and Tl/Ca for
637 clarity. The graph for K shows a non-zero intercept ($c \neq 0$).

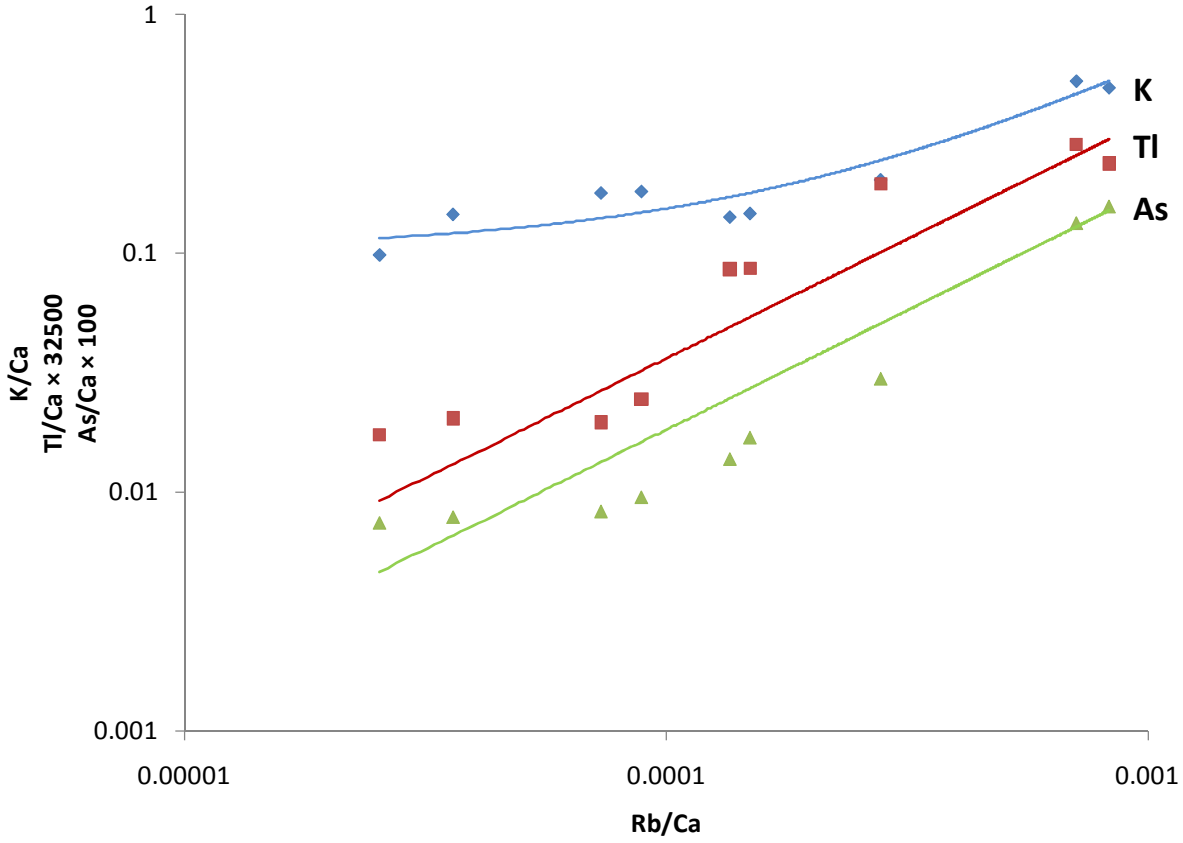

638

639

640 Figure 6A Correlation coefficients (R) between concentrations of elements
641 in Coirón grass and ash thickness at each location (T / mm).

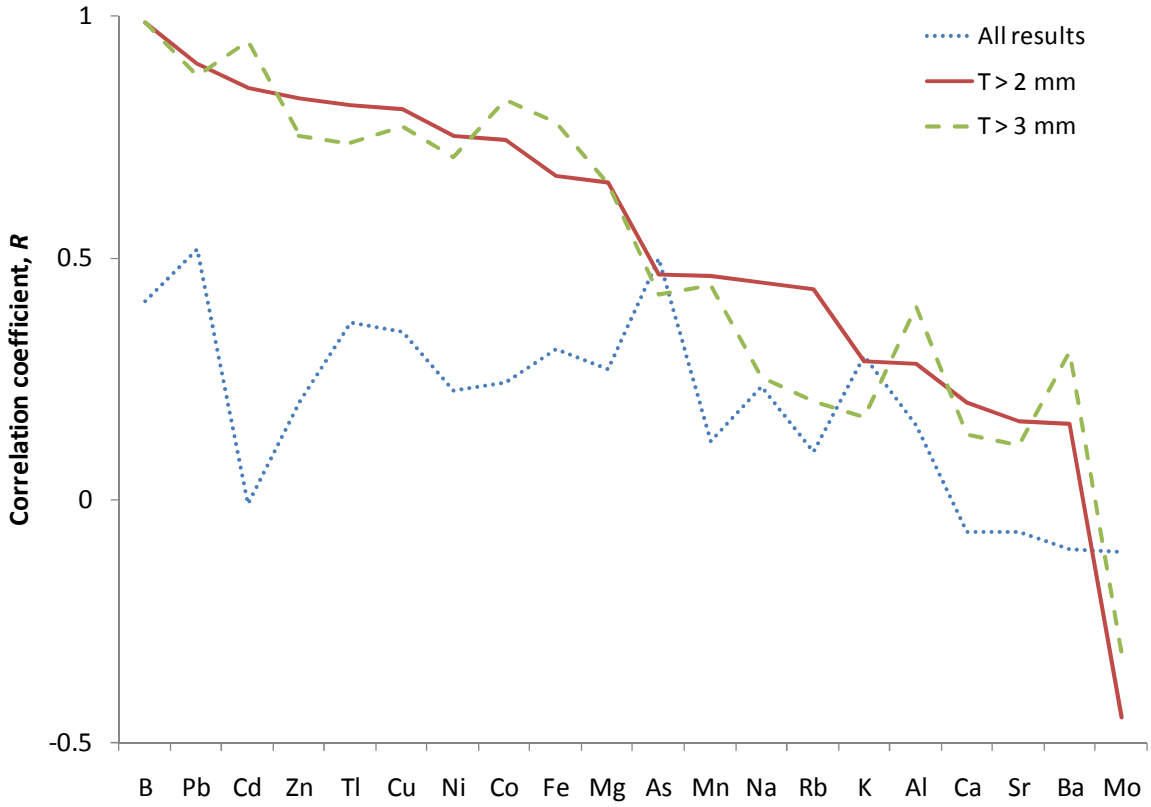

642

643

644 Figure 6B Concentrations of B, Pb and Cd in Coirón grass (ppm by mass) against ash
645 thickness at each location (T / mm). Samples where T > 2 mm are highlighted.

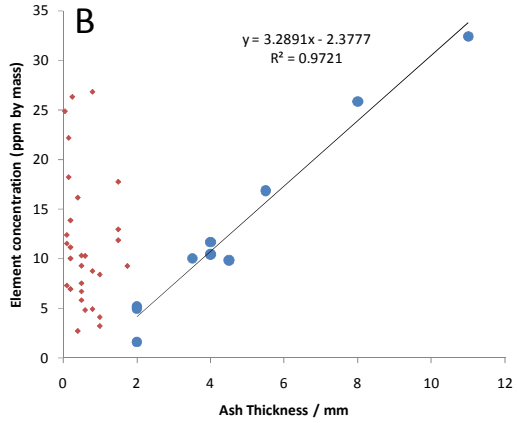

646

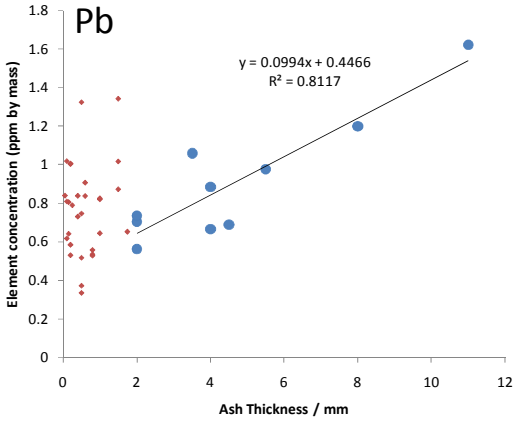

647

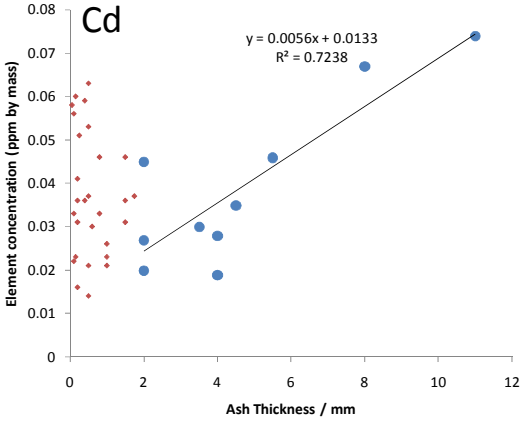

648

649

650 Figure 6C A comparison of correlation coefficients (R) between concentrations of elements
651 in Coirón grass and ash thickness at each location (T / mm) between June
652 2008($2 < T/\text{mm} < 6$) and January 2009 samples ($2.5 < T/\text{mm} < 6$).

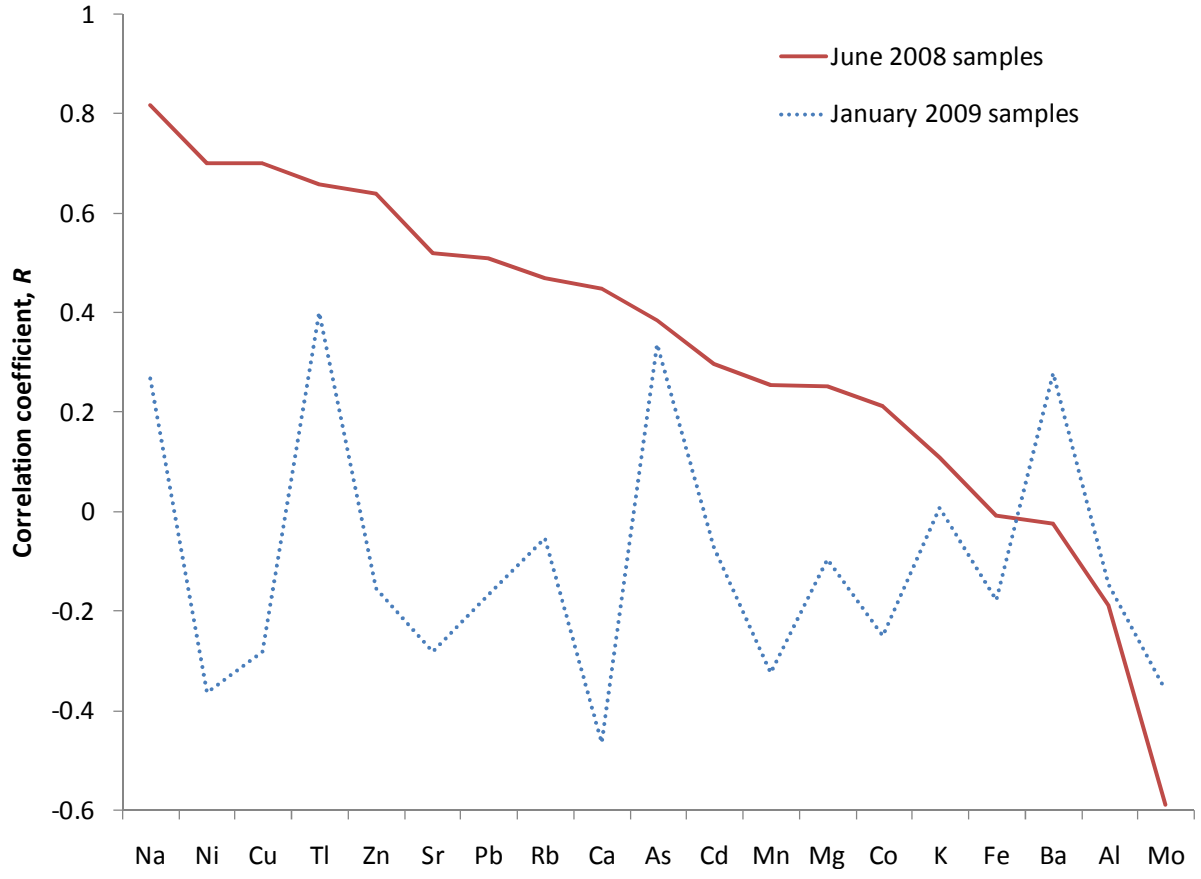

653

654

655 Table 1 Sample details for filter packs.

Sample	Date	Sampling Times (local time)	Duration (t / min)	Flow-rate (F / L min^{-1})	Volume (V_A / L)	Mass (M / mg)
04-01A	04/06/08	08:40-09:15	35	20	700	0.3
04-01B	04/06/08	09:30-10:15	45	19	855	0.9
04-01C	04/06/08	10:20-10:55	35	19	665	1.2
04-01D	04/06/08	11:10-11:45	35	19	665	1.1
04-01E	04/06/08	11:50-12:40	50	18	900	1.3
04-01F	04/06/08	12:42-13:22	40	19	760	0.7
04-01G	04/06/08	13:25-14:05	40	19	760	1.1
04-01H	04/06/08	14:10-14:55	45	19	855	0.9
04-01I	04/06/08	15:00-15:50	50	18	900	1.1
04-01J	04/06/08	15:55-16:48	53	18	954	0.6
04-01K	04/06/08	16:50-17:33	43	20	860	1.5
04-01M	04/06/08	17:45-18:43	58	18	1044	2.9
04-01N	04/06/08	18:47-12:47	180	15	2700	5
05-27A	05/06/08	09:00 -	-	-	-	12.5
07-01A	07/06/08	23:00 -	-	-	-	3.2

Samples taken on 5th and 7th June were left running unattended from the time indicated until the battery was exhausted. For these samples, V_A is unknown but is presumed common to both.

656

657

658 Table 2 $N(d_o = 4\ \mu m)$ for samples analysed using SEM.

659

660

Sample	$N(d_o = 4\ \mu m)$
04-01 D	7.5×10^6
04-01 E	7.1×10^6
04-01 H	9.4×10^6
04-01 I	7.3×10^6
04-01 M	6.9×10^6

661 Table 3 Estimates for element concentrations relative to Rb within the
662 soluble material on the surface of ash particles.

Element	Y/Rb
As	1.9
B	3.5
Cd	0.0012
Cl	780
Cs	0.013
Cu	0.14
Fe	2.2
K	510
Mn	1.2
Ni	0.27
Rb	1
Tl	0.00098
Zn	3.3

663

664

665 Supplementary Table 1 Sample details and data for lakes.

Sample Property	05-05	05-18	30-05	31-06	07-02	07-13	02-09
Latitude	-43.168	-43.528	-42.383	-43.325	-42.949	-42.138	-45.118
Longitude	-71.735	-71.204	-71.109	-70.896	-71.217	-71.018	-69.12
Ash thickness (T/mm)	15	9.5	3.5	3.5	2	0.4	0.1
Number of samples	2	1	2	2	2	1	1
Morphometry (m)	60×20×2	50×5×0.75	250×250×5	100×20×0.3	50×40×2	100×20×1	100×50×3
As	11	3	1.5	1.3	3.3	12	3.2
B	24	6.1	7.1	15	18	12	19
Ba	5.5	8.5	5.5	3.3	3.1	21	16
Ca	7400	10000	9400	15000	43000	32000	13000
Cd	0.0065	0.006	0.002	0	0	0	0
Co	0.044	0.045	0.055	0.084	0.19	0.41	0.1
Cs	0.079	0.041	0.017	0.048	0.019	0.063	0.009
Cu	0.89	0.47	0.27	0.07	0.29	0.73	0.21
Fe	23	18	14	28	60	66	19
K	3800	2000	1400	2700	5300	6100	970
Mg	1800	2600	2500	11000	9300	27000	420
Mn	6.6	3.4	1.8	1	1.9	8.9	4.8
Mo	0.33	0.55	0.48	0.45	0.56	2.8	0.77
Na	3700	4800	5200	19000	15000	36000	14000
Ni	1.9	1.1	0.74	0.6	1.2	3.1	0.77
Rb	5.7	2.8	1.4	1.2	1.3	6	0.43
Sr	26	37	40	88	97	140	20
Tl	0.006	0.006	0.0025	0.001	0.0025	0.01	0.002
Zn	19	7.1	1.9	1.7	2.4	8.3	0.27
Cl^-	5200	2300	2300	2400	3700	10000	5300
F^-	100	100	130	380	480	1200	200
SO_4^{2-}	3600	3000	2600	600	20000	15000	16000

Ash thickness (in mm) was measured as described in Watt et al., (2009). Lake morphometry was estimated and given as length × width × depth (in m). Element concentrations (determined by ICP-MS or IC) are given in units of ppb by mass.

666

667 Supplementary Table 2 Sample details for vegetation.

Sample	Collected	Latitude	Longitude	Ash Thickness (*T*) / mm
05-16	06/08	-43.488	-71.308	11
05-19	06/08	-43.561	-71.170	8
31-04	06/08	-43.015	-71.043	5.5
04-02	06/08	-43.063	-70.863	4.5
31-05	06/08	-43.134	-70.860	4
05-21	06/08	-43.609	-71.056	4
31-06	06/08	-43.325	-70.896	3.5
31-07	06/08	-43.528	-70.795	2
31-08	06/08	-43.640	-70.840	2
04-13	06/08	-42.960	-70.642	2
31-09	06/08	-43.797	-70.936	1.75
04-04	06/08	-43.035	-70.588	1.5
31-12	06/08	-44.046	-70.630	1.5
05-23	06/08	-43.585	-70.931	1.5
03-09	06/08	-43.467	-70.845	1
05-24	06/08	-43.559	-70.886	1
31-13	06/08	-44.177	-70.473	1
04-16	06/08	-42.656	-70.419	0.8
05-25	06/08	-43.513	-70.871	0.8
05-26	06/08	-43.474	-70.846	0.8
04-06	06/08	-43.075	-70.235	0.6
04-11	06/08	-43.089	-69.902	0.6
01-04	06/08	-43.727	-69.898	0.5
03-08	06/08	-43.573	-70.361	0.5
31-10	06/08	-43.959	-70.887	0.5
31-11	06/08	-43.994	-70.827	0.5
31-14	06/08	-44.292	-70.401	0.5
04-09	06/08	-43.214	-69.965	0.4
06-19	06/08	-41.968	-71.273	0.4
02-05	06/08	-44.646	-69.148	0.25
02-04	06/08	-44.459	-69.255	0.2
01-08	06/08	-43.672	-68.932	0.2
31-15	06/08	-44.419	-70.440	0.2
02-02	06/08	-44.146	-69.262	0.15
02-08	06/08	-45.035	-69.153	0.15
03-05	06/08	-43.950	-71.456	0.1
02-16	06/08	-45.448	-69.815	0.1
31-16	06/08	-44.589	-70.371	0.1
31-17	06/08	-44.731	-70.227	0.05
01-11	06/08	-43.877	-68.421	0.2
A-05	01/09	-42.004	-71.130	2.5 (0.2)
A-07	01/09	-41.841	-70.893	3 (0.2)
A-09	01/09	-42.384	-71.111	3 (0.5)
A-10	01/09	-42.467	-71.097	4 (1)
A-11	01/09	-42.659	-71.080	4 (2)
A-12	01/09	-42.767	-71.113	4 (1.5)
B-01	01/09	-42.969	-71.178	6 (3)
B-02	01/09	-43.050	-70.967	6(3)
B-03	01/09	-43.182	-70.845	4 (1)
B-04	01/09	-43.338	-70.886	3 (1)

For January 2009 samples, the ash thickness is given as the "original" ash thickness measured in June 2008 (Watt et al., 2009) followed by the remeasured ash thickness in parentheses.

668

669 Supplementary Table 3A Compositions of vegetation samples (ppm by mass)
670 determined by ICP-MS (for elements Al – K).

Sample	Al	As	B	Ba	Ca	Cd	Co	Cu	Fe	K
31-07	2100	0.21	1.6	7.8	2100	0.045	0.26	4.8	840	4900
31-10	520	0.055	5.9	3	940	0.014	0.081	1.8	220	980
05-26	720	0.11	27	7.4	6400	0.033	0.11	4.2	280	2700
03-09	3600	0.35	4.2	11	2500	0.023	0.38	4.3	1400	3400
02-08	3700	0.25	18	23	4500	0.023	0.32	3.8	1200	730
31-08	2200	0.2	5.2	12	1500	0.02	0.22	4.2	840	1700
03-05	1900	0.29	12	36	3400	0.022	0.2	7.2	760	2100
04-04	3600	0.27	12	13	3400	0.046	0.37	8.5	1500	1800
31-05	800	0.1	10	3.3	3300	0.028	0.11	9.2	300	7600
31-14	660	0.081	10	2.9	2300	0.021	0.089	6.3	280	6000
31-12	2500	0.26	13	12	3300	0.036	0.39	11	1200	2600
02-04	1200	0.12	7	17	2500	0.031	0.19	3.3	500	2200
31-09	930	0.062	9.3	8.4	1400	0.037	0.14	8.5	330	6900
04-13	3500	0.28	5	11	2900	0.027	0.34	4.3	1300	2600
01-08	1600	0.11	11	11	2000	0.036	0.27	13	660	3400
31-13	1900	0.16	3.3	7.1	1000	0.026	0.38	14	700	1800
05-23	1500	0.15	18	8.8	1900	0.031	0.25	12	650	2400
01-11	6900	0.32	10	37	5200	0.041	0.97	15	2800	3900
31-04	2500	0.51	17	13	4200	0.046	0.36	10	1200	3700
31-15	360	0.073	14	2.4	1900	0.016	0.51	6.6	170	5500
02-02	1900	0.12	22	17	2800	0.06	0.25	7.6	720	1500
04-06	3000	0.22	10	9.9	1800	0.31	0.37	4.4	1200	3200
31-11	6300	0.33	9.3	16	3100	0.063	0.53	8.7	2400	3600
31-16	1000	0.16	7.3	6.2	2200	0.056	0.12	5.4	450	2100
31-17	1100	0.14	25	6	1600	0.058	0.14	7.5	470	2100
31-06	1400	0.13	10	5.3	1100	0.03	0.13	5.7	530	4900
04-09	2400	0.2	16	9.3	2500	0.036	0.3	7.8	880	3700
04-16	2000	0.19	5	4.9	3300	0.046	0.25	5.6	780	2800
03-08	320	0.066	7.6	1.6	1700	0.053	0.059	2.8	130	2200
05-25	1100	0.18	8.8	5.9	3300	0.32	0.14	3.2	460	3800
02-05	790	0.059	26	3.6	2400	0.051	0.19	9.8	430	3200
05-16	2000	0.27	32	7	2000	0.074	0.53	19	1700	6100
05-21	2400	0.32	12	10	1700	0.019	0.27	4	930	2300
05-24	1600	0.14	8.4	9.9	1500	0.021	0.27	6.1	680	1700
04-11	1800	0.37	4.9	21	3900	0.03	0.2	6.9	760	5100
01-04	3000	0.39	6.7	8.7	3800	0.037	0.47	6.4	1600	2300
05-19	5800	1.1	26	18	3200	0.067	0.58	5.7	2400	3000
06-19	2900	0.29	2.8	12	1900	0.059	0.32	5.9	1200	3900
02-16	3100	0.19	12	13	3600	0.033	0.35	5	1400	3500
04-02	2500	0.16	9.9	8.6	2000	0.035	0.38	5.5	970	1700
A-05	590	0.19	-	5.2	4600	0.02	0.31	7	660	5800
A-07	550	0.67	-	4.2	3300	0.019	0.31	5.3	770	3900
A-09	890	0.47	-	11	10000	0.027	0.39	7.9	890	6600
A-10	270	0.17	-	6.3	3900	0.1	0.14	5	280	4900
A-11	180	0.13	-	4	2800	0.015	0.098	3.8	200	4200
A-12	320	0.22	-	7.7	3400	0.034	0.18	5.1	320	3900
B-01	980	1.1	-	12	3900	0.028	0.42	8.2	1100	8100
B-02	230	0.33	-	6.8	3000	0.012	0.14	3	290	3000
B-03	280	0.3	-	2.4	3600	0.018	0.16	3.8	340	4700
B-04	830	0.5	-	7.7	8500	0.04	0.43	7.3	990	5400

671

672 Supplementary Table 3B Compositions of vegetation samples (ppm by mass)
673 determined by ICP-MS (for elements Mg – Zn)

Sample	Mg	Mn	Mo	Na	Ni	Pb	Rb	Sr	Tl	Zn
31-07	630	40	1.8	180	0.85	0.56	0.9	11	0.01	11
31-10	250	13	0.57	60	0.43	0.37	0.29	6.3	0.008	10
05-26	610	110	1.8	160	0.62	0.54	0.57	26	0.01	11
03-09	720	59	0.53	380	1.1	0.82	2.3	15	0.014	11
02-08	470	43	7.8	730	0.92	0.81	1.7	16	0.013	5.6
31-08	390	22	0.84	220	0.64	0.7	0.94	10	0.012	9.3
03-05	880	21	0.18	320	0.81	1	2.1	26	0.014	13
04-04	490	38	1.8	310	1.5	1	1.6	9.5	0.018	9.9
31-05	880	35	0.62	240	1.1	0.88	2.4	6	0.017	22
31-14	710	22	0.29	95	0.76	0.52	0.88	7.2	0.009	9.6
31-12	550	33	1.3	450	1.7	0.87	1.3	26	0.019	18
02-04	470	18	0.32	170	0.85	0.59	0.95	10	0.012	21
31-09	900	12	3.2	180	1.1	0.65	1.5	10	0.011	11
04-13	640	35	2.8	210	0.81	0.73	1.5	14	0.013	9
01-08	420	36	1.7	160	0.87	1	1.7	13	0.015	16
31-13	320	20	0.77	230	0.6	0.83	0.92	5.9	0.011	11
05-23	430	19	0.57	260	1	1.3	1.1	10	0.016	15
01-11	1200	90	1.5	580	3.1	1	3.1	56	0.022	25
31-04	670	34	0.61	520	1.6	0.98	1.7	37	0.02	18
31-15	340	18	0.45	81	0.69	0.53	0.63	6	0.01	12
02-02	400	30	1.6	230	0.97	0.64	1.2	18	0.015	15
04-06	540	38	0.81	230	2.9	0.91	1.4	9.9	0.013	14
31-11	810	50	1.6	210	1	1.3	2.3	18	0.021	17
31-16	450	19	0.85	120	0.65	0.62	0.58	13	0.011	8.6
31-17	310	22	0.47	170	1	0.84	0.77	10	0.015	11
31-06	530	11	2	270	0.83	1.1	1.3	5	0.014	13
04-09	550	30	1.1	250	1.4	0.73	1.5	14	0.018	47
04-16	680	36	1.1	280	1	0.53	1	14	0.011	8.5
03-08	270	12	0.91	69	0.49	0.34	0.61	6.2	0.008	5.8
05-25	590	82	1.6	180	0.54	0.56	0.67	13	0.009	7.3
02-05	580	26	0.78	190	2.9	0.79	0.98	11	0.013	39
05-16	890	45	0.85	230	2.7	1.6	1.4	9.6	0.021	32
05-21	390	30	1.4	230	0.53	0.66	1.2	11	0.011	11
05-24	420	23	0.89	190	1.5	0.65	0.79	9.1	0.011	9.9
04-11	1100	21	0.78	540	0.99	0.84	5.9	26	0.015	16
01-04	790	34	2.4	570	1.1	0.75	1.8	34	0.019	13
05-19	860	57	1.2	780	0.8	1.2	2.8	17	0.019	16
06-19	400	41	3.1	130	0.63	0.84	2.8	9.5	0.011	13
02-16	770	43	2.7	540	0.76	0.81	1.3	19	0.016	13
04-02	600	63	1.1	320	1.6	0.69	1.3	11	0.012	12
A-05	1400	45	1.3	110	0.82	0.8	3	16	0.0065	12
A-07	700	23	2.8	170	1	0.65	1.1	9.4	0.016	6
A-09	530	31	1.8	170	0.89	1.3	1.6	33	0.016	13
A-10	370	47	0.94	76	0.66	0.58	1.7	15	0.0079	19
A-11	570	24	1.3	83	0.98	0.58	1.7	11	0.0071	11
A-12	690	61	5	110	0.86	0.66	0.9	13	0.01	11
B-01	900	32	0.53	260	1.1	1.1	2.9	16	0.03	12
B-02	760	24	0.96	110	0.45	0.58	0.74	13	0.0095	5.2
B-03	350	17	1.7	83	0.61	0.81	0.59	11	0.0096	5.7
B-04	690	80	2.3	140	1.5	1	1.4	22	0.014	10

674